



## OPEN ACCESS

## EDITED BY

Talia Karasov,  
The University of Utah, United States

## REVIEWED BY

Saowarat Jantaro,  
Chulalongkorn University, Thailand  
Pia Lindberg,  
Uppsala University, Sweden

## \*CORRESPONDENCE

Ilka M. Axmann  
[ilka.axmann@hhu.de](mailto:ilka.axmann@hhu.de)

<sup>†</sup>These authors have contributed  
equally to this work and share  
first authorship

RECEIVED 22 August 2022

ACCEPTED 28 April 2023

PUBLISHED 30 May 2023

## CITATION

Germann AT, Nakielski A, Dietsch M, Petzel T, Moser D, Triesch S, Westhoff P and Axmann IM (2023) A systematic overexpression approach reveals native targets to increase squalene production in *Synechocystis* sp. PCC 6803. *Front. Plant Sci.* 14:1024981. doi: 10.3389/fpls.2023.1024981

## COPYRIGHT

© 2023 Germann, Nakielski, Dietsch, Petzel, Moser, Triesch, Westhoff and Axmann. This is an open-access article distributed under the terms of the [Creative Commons Attribution License \(CC BY\)](#). The use, distribution or reproduction in other forums is permitted, provided the original author(s) and the copyright owner(s) are credited and that the original publication in this journal is cited, in accordance with accepted academic practice. No use, distribution or reproduction is permitted which does not comply with these terms.

# A systematic overexpression approach reveals native targets to increase squalene production in *Synechocystis* sp. PCC 6803

Anna T. Germann<sup>1†</sup>, Andreas Nakielski<sup>1†</sup>, Maximilian Dietsch<sup>1</sup>, Tim Petzel<sup>1</sup>, Daniel Moser<sup>2</sup>, Sebastian Triesch<sup>3</sup>, Philipp Westhoff<sup>4</sup> and Ilka M. Axmann<sup>1\*</sup>

<sup>1</sup>Institute for Synthetic Microbiology, Department of Biology, Heinrich Heine University Düsseldorf, Düsseldorf, Germany, <sup>2</sup>Institute for Plant Sciences and Cluster of Excellence on Plant Sciences (CEPLAS), University of Cologne, Cologne, Germany, <sup>3</sup>Institute of Plant Biochemistry, Cluster of Excellence on Plant Science (CEPLAS), Heinrich Heine University, Düsseldorf, Germany, <sup>4</sup>Plant Metabolism and Metabolomics Laboratory, Cluster of Excellence on Plant Sciences (CEPLAS), Heinrich Heine University Düsseldorf, Düsseldorf, Germany

Cyanobacteria are a promising platform for the production of the triterpene squalene (C<sub>30</sub>), a precursor for all plant and animal sterols, and a highly attractive intermediate towards triterpenoids, a large group of secondary plant metabolites. *Synechocystis* sp. PCC 6803 natively produces squalene from CO<sub>2</sub> through the MEP pathway. Based on the predictions of a constraint-based metabolic model, we took a systematic overexpression approach to quantify native *Synechocystis* gene's impact on squalene production in a squalene-hopene cyclase gene knock-out strain ( $\Delta shc$ ). Our *in silico* analysis revealed an increased flux through the Calvin-Benson-Bassham cycle in the  $\Delta shc$  mutant compared to the wildtype, including the pentose phosphate pathway, as well as lower glycolysis, while the tricarboxylic acid cycle predicted to be downregulated. Further, all enzymes of the MEP pathway and terpenoid synthesis, as well as enzymes from the central carbon metabolism, Gap2, Tpi and PyrK, were predicted to positively contribute to squalene production upon their overexpression. Each identified target gene was integrated into the genome of *Synechocystis*  $\Delta shc$  under the control of the rhamnose-inducible promoter P<sub>rha</sub>. Squalene production was increased in an inducer concentration dependent manner through the overexpression of most predicted genes, which are genes of the MEP pathway, *ispH*, *ispE*, and *idi*, leading to the greatest improvements. Moreover, we were able to overexpress the native squalene synthase gene (*sqs*) in *Synechocystis*  $\Delta shc$ , which reached the highest production titer of 13.72 mg l<sup>-1</sup> reported for squalene in *Synechocystis* sp. PCC 6803 so far, thereby providing a promising and sustainable platform for triterpene production.

## KEYWORDS

*Synechocystis*, squalene, MEP pathway, FBA, metabolic engineering, metabolic modeling

## Introduction

Cyanobacteria are the only known prokaryotes capable of oxygenic photosynthesis (Mul�idjanian et al., 2006; Lau et al., 2015). The gram-negative bacteria exhibit a large ecological variety as well as a broad morphological diversity (Bennett and Bogorad, 1973; Rippka et al., 1979; Schirrmeyer et al., 2013). Their physiological diversity makes them promising biological chassis for the synthesis of a variety of natural products, including bioactive metabolites like cytotoxins and potential pharmaceutical lead compounds, food supplements, animal feed, pigments, as well as biofuels (Pulz and Gross, 2004; Hays and Ducat, 2015; Jain et al., 2017; Hudson et al., 2021; Barone et al., 2023). Their ability to convert sunlight and atmospheric CO<sub>2</sub> directly into valuable organic compounds could make the chemical and pharmaceutical industry more sustainable and therefore mitigate climate change if high production yields are achieved (Choi et al., 2020; Posten and Schaub, 2009; Oliver and Atsumi, 2015; Oliver et al., 2016).

Metabolic engineering tools for the production of desired compounds are particularly well established for laboratory model strains like *Synechocystis* sp. PCC 6803 (hereafter *Synechocystis*) (Knoop and Steuer, 2015; Ramey et al., 2015). The unicellular organism was the first entirely sequenced cyanobacterium (Kaneko et al., 1996) and is one of the best characterized model organisms regarding cyanobacterial biosynthesis (Pils and Schmetterer, 2001; Leplat et al., 2013). *Synechocystis* is easy and inexpensive to cultivate, and is genetically modifiable with high success rates and predictability (Rippka et al., 1979; Berla et al., 2013).

One promising class of compounds to be produced in cyanobacteria are terpenoids, a large heterogeneous group of naturally occurring organic carbon compounds with over 80,000 known structures (Karunanithi and Zerbe, 2019), having applications in nutrition, medicine and chemistry but also as potential biofuels. Triterpenoids are a group of secondary metabolites, which are composed of 6 isoprene units (Moss et al., 1995), existing in a huge variety of structures with nearly 200 distinct triterpene skeletons, all deriving from the precursor squalene (Xu et al., 2004; Connolly and Hill, 2010). Squalene is typically extracted from shark liver oil, but this method poses serious ecological risks and is not sufficient to sustainably meet increasing demands (Gohil et al., 2019; O'Hagan et al., 2021; Mendes et al., 2022). The diverse applications of squalene include its use as an ingredient in cosmetic products (Gohil et al., 2019), as an antioxidant (Kohno et al., 1995) and an emulsion adjuvant in vaccines (O'Hagan et al., 2021). It has recently been used in several COVID-19 vaccines (Liang et al., 2020; Ho et al., 2021), introducing a surge in demand for this terpenoid. Other reported properties of squalene include tumor-suppressing (Smith et al., 1998; Yang et al., 2014), immunity improving (Ronco and De Stéfani, 2013), cholesterol-lowering (He et al., 2003), as well as antibacterial and antifungal effects (Katabami et al., 2015). Squalene has attracted attention as a feasible source of biofuels (Hellier et al., 2013) as well, if it could be produced sustainably and in large quantities.

In most plants, algae and prokaryotes, terpenoids can be synthesized via the methyl-erythritol-4-phosphate (MEP) pathway,

also called the non-mevalonate pathway (Okada and Hase, 2005; Sawai and Saito, 2011). While the mevalonate pathway is present in most eukaryotic cells, the MEP pathway was acquired through endosymbiotic or horizontal gene transfer in plastid-bearing organisms. As the progenitors of plastids, cyanobacteria can serve as both a model organism for chloroplastic terpenoid synthesis through the MEP pathway and are promising production hosts for plant terpenoids (Hemmerlin et al., 2006; Loeschke et al., 2017). The MEP pathway produces isopentenyl diphosphate (IPP) and dimethylallyl diphosphate (DMAPP), which are the universal precursors for terpenoid synthesis. In *Synechocystis*, a single gene, *crtE*, is responsible for the elongation of terpene precursors towards geranyl pyrophosphate (GPP), farnesyl pyrophosphate (FPP) and geranylgeranyl pyrophosphate (GGPP) in consecutive condensation reactions. The enzyme squalene synthase (Sqs) catalyzes the condensation of two molecules of FPP to presqualene diphosphate (PSPP), which is then converted into squalene via reduction by NADPH. In *Synechocystis*, squalene is then cyclized by squalene hopene cyclase (Shc) to hopene (Englund et al., 2014). Englund and colleagues (Englund et al., 2014) used a modified strain of *Synechocystis* to produce squalene by inactivating the *shc* gene. By preventing the generation of hopene, squalene is accumulated in this mutant. We previously constructed a markerless deletion of *shc* in *Synechocystis* to minimize the number of antibiotic resistances carried by each strain and enable further engineering (Dietsch et al., 2021). The availability of inducible promoter systems, such as the rhamnose, anhydrotetracycline or copper inducible promoters in *Synechocystis* allows fine-tuning of gene expression levels, making improvement of metabolic pathways possible by identifying optimal expression levels for each involved gene (Behle et al., 2020).

A straightforward approach to achieve higher yields of desired products is the overexpression of certain genes to increase the flux towards these metabolites, with many strategies already reported for increasing heterologous terpenoid production (Klaus et al., 2022). Despite some strategies proving successful, the regulation and bottlenecks of the MEP pathway are still not entirely understood (Klaus et al., 2022). Most initial pathway modification approaches result in relatively low product yield, and optimization is often dependent on heuristic techniques (Choi et al., 2017; Steuer et al., 2012). While the identification of genes to be modified is an essential step in metabolic engineering for strain improvement toward the enhanced production of desired bioproducts, it is still difficult to decide which genes to insert or modify, due to the vast number of possibilities of potential targets and the consideration of complex regulation of metabolic networks. In order to rationally identify and overcome bottlenecks for the improvement of strain designs, the use of *in silico* models has gained increasing significance over the past years (King et al., 2015; Brodrick et al., 2016; Lin et al., 2017; Hendry et al., 2020). Genome-scale metabolic modeling requires only stoichiometric information and no kinetic parameters, which are usually not available even for small reaction networks. In contrast, stoichiometric information is readily and reliably available for a large number of annotated genes (Raman and Chandra, 2009). Additionally, the estimation of stoichiometric yield is computationally not expensive and feasible even for large models involving hundreds of reactions (Knoop and Steuer, 2015).

Constraint-based reconstruction and analysis (COBRA) utilizes these models to calculate flux distributions under certain environmental or internal conditions (Schellenberger et al., 2011). COBRA methods are mainly used for the prediction of maximum theoretical yield for native and non-native pathways (Shen and Liao, 2013; King et al., 2015), the effect of gene deletions on biomass or other target compounds (e.g. OptKnock) (Burgard et al., 2003) as well as the identification of bottlenecks and potential targets for up- and downregulation in order to increase product yield (e.g. flux scanning based on enforced objective flux (FSEOF) or minimization of metabolic adjustment (MOMA)) (Segré et al., 2002; Choi et al., 2010). Previous studies (Choi et al., 2010; Englund et al., 2018; Park et al., 2018), aiming to increase terpenoid production, have shown that constraint-based flux balance analysis (FBA) can be a helpful tool to not only understand and analyze metabolic pathways, but to identify bottlenecks and narrow down the options of potential amplification or knock-down targets for increased product yield, without having a negative influence on the growth rate. Englund et al. successfully employed genome-scale metabolic flux analysis to identify amplification targets that increased isoprene production in *Synechocystis* (Englund et al., 2018).

In our work, we used an algorithm called FSEOF to screen for potential overexpression targets increasing the terpenoid concentration in *Synechocystis* (Choi et al., 2010). *In silico* analysis predicted an increased flux through reactions of the MEP pathway, terpenoid synthesis, the light-dependent reactions of photosynthesis as well as the central carbon metabolism. Additionally, metabolic modeling proposed elevated requirements for the efficient supply, balance and regeneration of cofactors. Twelve of the identified amplification targets were tested *in vivo* to assess the biological relevance of the model, all of which positively impacted squalene production. The overexpression of *sqs* led to the strongest increase, with a yield of 13.72 mg l<sup>-1</sup>, the highest production titer reported for squalene in *Synechocystis* to date.

## Materials and methods

### Plasmid and strain construction

A detailed list of all relevant genetic modules and information regarding their origin, is provided in the Supporting Information (Table S1 (SI)).

To investigate the computationally identified genes' effect on squalene production, the pEERM4 plasmid was used to integrate each gene into the neutral site 2 (NS2) under control of the rhamnose promoter P<sub>rha</sub> (Englund et al., 2015; Behle et al., 2020). The plasmid pEERM4 Cm was a gift from Pia Lindberg (Addgene plasmid # 64026; <http://n2t.net/addgene:64026>; RRID : Addgene\_64026) (Englund et al., 2015). This plasmid was used to clone each gene of interest under the control of P<sub>rha</sub>. It contains 500 bp DNA homologous to the upstream and downstream region of NS2, between which a chloramphenicol resistance and the gene of interest are located, flanked by the rhamnose promoter and the T7 terminator. Each gene of interest was cloned into the plasmid using

the restriction enzymes NheI and PstI, with the NheI cutting site located after the start codon. The genes of interest were amplified from the *Synechocystis* genome, using Q5-Polymerase (NEB # M0491) according to manufacturer's instructions with oligonucleotides shown in Table S2 (SI). In two cases, an NheI restriction site was removed from the native gene sequence without changing the amino acid sequence (*gap2*, *sqs*). The *sqs* gene is annotated as starting with GTG as a start codon in the published Kazusa genome and this codon was changed to ATG for the purposes of this study.

To enable induction of the P<sub>rha</sub> promoter, the rhamnose activator *rhaS* was constitutively expressed by the J23119 promoter from the replicative plasmid pSHDY (AddGene Plasmid #137661, (Behle et al., 2020)), which was transferred to *Synechocystis* via triparental mating (Behle et al., 2020). This plasmid was constructed using the restriction sites of the BioBrick and NeoBrick standards and carries a spectinomycin resistance.

*Synechocystis* was transformed with the pEERM4 plasmids (Table S1 (SI)) using a protocol based on its natural competence (dx.doi.org/10.17504/protocols.io.mdrc256). Successful integration of the plasmid into the genome through heterologous recombination into the neutral site 2 (NS2) (Satoh et al., 2001) was verified by colony PCR (Figure S1 (SI)). The plasmid pSHDY carrying the rhamnose activator *rhaS* was then transferred to *Synechocystis* using triparental mating (dx.doi.org/10.17504/protocols.io.psndne).

### Culture conditions

The *Synechocystis* strains were inoculated in 30 ml BG11 liquid cultures containing 20 µg/ml spectinomycin and for overexpression strains 10 µg/ml chloramphenicol in 100 ml Erlenmeyer flasks from agar plates. The cultures were diluted twice to an OD<sub>750</sub> of 0.2 to equalize their cell densities and growth phases. Two days before the start of the experiment, cultures were again diluted to an OD<sub>750</sub> of 0.2 after which they were transferred to 6-well plates with 5 ml per well. L-Rhamnose was then added to the cultures and they were grown for 72 h at 30°C with 150 rpm shaking, 0.5% CO<sub>2</sub> and 80 µE m<sup>-2</sup> s<sup>-1</sup> of continuous light. After 72 h, cell samples were taken and stored for further processing.

For measurements of squalene production over time, 30 ml of BG11 were inoculated from a pre-culture to OD<sub>750</sub> = 0.4, supplemented with 5 mM of rhamnose and incubated over 14 days. Samples were taken daily for the first four days, every second day for the following six days and after 14 days. The lost culture volume from sampling was replaced with fresh BG11 containing appropriate antibiotics and 5 mM of rhamnose.

### Biomass measurements (DCW, OD, spectra)

Cell dry weight measurements were carried out by transferring the cell pellet of 2 ml of cyanobacterial culture to a pre-weighed

PCR tube, which was incubated at 60°C for 20 h. The tube was weighed and the difference noted as the cell dry weight, with measurements carried out in triplicates.

Absorption spectra and OD measurements were carried out in 1 ml polystyrene cuvettes in a SPECORD 200 Plus Spectrophotometer (Analytik Jena) with BG11 as a blank and as a reference sample. Samples were diluted with BG11 to be within an absorption range of 0.1 to 1.0 to ensure accurate measurements. Cell densities for *Synechocystis* were measured at 750 nm.

## Pigment quantification

Each culture (300 µL) was sampled after 72 hours at the end of the growth experiment. The sample was centrifuged at 14,000 g for 5 minutes and 4°C. The supernatant was discarded and the pellet was resuspended in 100 µL water. The samples were frozen at -80°C until further processing. 900 µL of 100% methanol were added to the sample and the sample was mixed by vortexing. After incubation in the dark under gentle agitation for 1 h at 4°C the sample was centrifuged at 14,000 g for 5 minutes. The supernatant was transferred into a cuvette and an absorbance spectrum was measured from 400 nm to 750 nm. The absorbance spectra were divided by the OD<sub>750</sub> or CDW and the amount of chlorophyll *a* in the sample was quantified by the absorbance maximum of chlorophyll *a* at 665 nm (A<sub>665nm</sub>) using following equation (Lichtenthaler and Buschmann 2001):

$$\text{Chlorophyll content}[\mu\text{g}/\text{ml}] = 12.66 \mu\text{g}/\text{ml} \cdot A_{665 \text{ nm}}$$

The amount of carotenoids in the sample was quantified by the absorbance maximum of the sum of carotenoids at 470 nm (A<sub>470nm</sub>) and a correction term considering absorbance of chlorophyll *a* at 470 nm (c(Chl *a*): concentration of chlorophyll *a* in the sample) using following Equation (Lichtenthaler and Buschmann 2001):

$$\begin{aligned} \text{Carotenoid content}[\text{mg}/\text{ml}] \\ = (1000 \mu\text{g}/\text{ml} \cdot A_{470 \text{ nm}} - 1.91 \cdot c(\text{Chl})) / 225 \end{aligned}$$

## GC-MS measurements for the quantification of squalene

Each culture (1.5 ml) was sampled after 72 hours at the end of the growth experiment. The sample was centrifuged at 14,000 g, for five minutes and 4°C. The supernatant was discarded and the pellet was frozen at -80°C until further processing. The pellet was extracted with 500 µL acetone, containing 25 µM β-sitosterol as internal standard, under agitation at 1000 rpm and 50°C for 10 min. 500 µL of 1 M NaCl was added and mixed by vortexing. After adding 250 µL hexane, the sample was vigorously mixed for 1 min and centrifuged for phase separation (1 min at 1,780 g and 4°C). The upper hexane phase was transferred into GC-MS vials and stored at -20°C until the analysis.

GC-MS analysis was carried out using a Gerstel automatic liner exchange system with multipurpose sample MPS2 dual rail and two derivatization stations, used in conjunction with a Gerstel CIS cold

injection system (Gerstel, Muehlheim, Germany). For every 10-12 samples, a fresh multibaffled liner was inserted. Chromatography was performed using the Agilent 7890B GC. Metabolites were separated on an Agilent HP-5MS column (30ml x 0.25mm), the oven temperature was ramped with 12.5 °C/min from 70 °C (initial temp for 2 min) to 320 °C (final temp hold 5 min). Metabolites were ionized and fragmented in an EI source (70V, 200 °C source temp) and detected using 7200 accurate mass Q-TOF GC-MS from Agilent Technologies. Data analysis was performed using Agilent MassHunter Quantitative Analysis B.09.00. Peaks were identified using already available EI-MS fragmentation data. Peaks were identified using characteristic fragment ions (Bhatia et al., 2013) and retention times of standards (Squalene: mass/charge (m/z) = 81.07, retention time (RT) = 9.5 min; β-sitosterol: m/z = 107.09, RT = 13.6 min). Squalene concentrations in the measured samples were calculated using a calibration curve with a squalene standard (Figure S2 (SI)).

## Quantitative real-time PCR (qRT-PCR)

Cultures were sampled (0.5 ml) after 72 hours at the end of the growth experiment. The pellet was processed for RNA extraction using the PGTx method (dx.doi.org/10.17504/protocols.io.jm3ck8n, Pinto et al., 2009). The remaining DNA in the extracted RNA was removed by DNase digestion using the TURBO DNA-free™ (ThermoFischer) kit according to the manufacturer's instructions. Extracted RNAs (250 ng) were used in a reverse transcriptase reaction using the RevertAid First Strand cDNA Synthesis Kit (ThermoFischer) according to the manufacturer's instructions. The resulting cDNA was diluted 1:20. For performing qPCR, the DyNAamo ColorFlash SYBR Green qPCR Kit was used according to the manufacturer's instructions. Primers for *sqs*, *dxs* and the housekeeping gene *rpoA* are shown in Table S2 (SI). Primer efficiencies were tested before performing qRT-PCR and were deemed sufficient to yield quantitative information (Figure S3; Table S3 (SI)). Changes in gene expression as fold changes compared to the control were determined using the 2<sup>-ΔΔCT</sup> method, using *rpoA* as a housekeeping gene and the Δshc strain subjected to the same rhamnose concentration as a control.

## Metabolic modeling for the identification of amplification targets

All simulations are based on a genome-scale stoichiometric network model of *Synechocystis* published by Knoop and colleagues (Knoop and Steuer, 2015). A modified, extended version was used, kindly provided by Ralf Steuer. All flux distributions have been calculated with constraint-based flux analysis using COBRApy (v.0.25.0) (Ebrahim et al., 2013). To simulate phototrophic growth, different constraints were applied to the model of *Synechocystis* (see Table S5 (SI)).

FSEOF (Choi et al., 2010) was used to find amplification targets by simulating the transition from a wildtype to a production phenotype. All isoreactions were excluded for the transition experiments (Knoop and Steuer, 2015). The initial fluxes of all

reactions were calculated by using the objective function to maximize the growth rate. Then, the theoretical maximum squalene production rate was calculated by setting the objective function as maximizing squalene flux. Subsequently, under constant light flux, the product formation flux rate was stepwise increased from 0% to 67% of the maximum achievable rate, while the growth rate was maximized. Only targets for which the overall mean flux rate from maximum biomass synthesis to maximum product synthesis increases were chosen. Additionally, only reactions that did not change flux direction during transition were considered. To confirm the results, flux variability analysis was performed for the selected targets, by stepwise increasing squalene flux from 0% to 67% of the maximum rate and subsequently maximizing biomass synthesis. For each simulation step, the variability of all selected targets was determined. To visualize the flux distributions a simplified network was implemented with d3flux (v.0.2.7) (St. John, 2016), a d3.js based visualization tool for COBRApy models.

## Results

### Metabolic modeling predicts overexpression targets in MEP pathway and central carbon metabolism

In this study our goal was to enhance squalene production by identifying potential amplification targets and systematically overexpressing selected genes of interest. Due to the extensive number of possible genes to modify, we chose to first screen for suitable targets *in silico*. We used a genome-scale metabolic network of *Synechocystis* to find the ideal flux distribution for the optimal production of squalene while maintaining at least 1/3 of the growth rate. Reactions that increase in flux, when more squalene is produced, were chosen as potential amplification targets.

To predict these targets, we applied an algorithm called FSEOF, developed by Choi and colleagues (Choi et al., 2010). The transition from a wildtype phenotype to a production phenotype was simulated by stepwise increasing squalene flux while the growth rate was maximized. This way, all resources beyond the growth rate are directed towards the forced product synthesis. We only considered targets for which the overall mean flux rate increases and that did not change flux direction during transition (Knoop and Steuer, 2015). An overview of reactions meeting these criteria can be found in Figure 1 and in Table S6 (SI). Excluding transport, export and spontaneous reactions, 39 potential overexpression targets were identified. Flux variability analysis was performed for these targets to validate the results (Table S7 (SI)). Upon enforced objective flux different flux patterns could be observed. 22 fluxes showed an increasing pattern without any variability. Among the remaining fluxes two increased within a narrow range and seven increased with broad variability. Three showed a pattern, where the minimal flux increased and the maximum possible flux decreased. One reaction showed a pattern indicating a change in flux direction and four were unbound.

The results of the metabolic modeling suggest an increase of flux through the MEP pathway, from the decarboxylative carboligation of glyceraldehyde 3-phosphate (G3P) and pyruvate to deoxyxylulose 5-

phosphate (DXP) by deoxyxylulose 5-phosphate synthase (Dxs), to the formation of isopentenyl diphosphate (IPP) by IspH as well its conversion to DMAPP by isomerization (Idi). The following reactions towards terpenoid synthesis, catalyzed by CrtE and Sqs, are also showing a flux increase.

Additionally, the model suggests an increased flux through cytidine monophosphate kinase (CMPk) and cytidine diphosphate kinase (CDPk) as well as an increased activity of inorganic diphosphatase (Ppa), converting diphosphate to monophosphate.

The reactions of lower glycolysis are proposed to be upregulated as well. 3-Phospho-D-glycerate (PG3), obtained by the RuBisCO reaction, is converted to 2-phospho-D-glycerate (PG2) by phosphoglycerate mutase (Pgm), to phosphoenolpyruvate (PEP) by enolase (Eno) and finally to pyruvate by pyruvate kinase (PyrK).

To provide the carbon needed for enhanced terpenoid synthesis, the total flux through the Calvin-Benson-Bassham (CBB) cycle is expected to increase. Especially the flux through RuBisCO, fixing CO<sub>2</sub> as PG3 shows a strong increase. The same applies to the phosphorylation of PG3 to 1,3-bisphosphoglycerate (13DPG) by phosphoglycerate kinase (PgK), its reduction to the MEP pathway precursor G3P by glyceraldehyde 3-phosphate dehydrogenase (Gap2), the conversion to dihydroxyacetone-phosphate (DHAP) by triosephosphate isomerase (Tpi) as well as the subsequent regeneration of D-ribulose 1,5-bisphosphate (RuDP) through the reductive pentose phosphate pathway.

The model predicts an increased flux through the light-dependent reactions of oxygenic photosynthesis in the thylakoid membrane. However, photosynthetic pigments like chlorophyll and carotenoids display a reduced flux. Whereas NADPH production via ferredoxin-NADP<sup>+</sup> reductase (FNR) is suggested to be increased, ATPase activity is supposed to be decreased. This goes along with a reduced TCA cycle activity.

As enhanced flux through the light reactions and CBB cycle are predicted, photorespiratory metabolism increases as well. However, the model suggests utilizing the glycerate photorespiratory bypass via tartronate semialdehyde. Phosphoglycolate as an inevitable by-product of the photorespiratory chain is converted to first glycolate, then glyoxylate, tartronate semialdehyde and afterwards to glycerate, which can be used to synthesize pyruvate or be recycled into the CBB cycle.

In summary, the model proposes an increased flux through the MEP pathway and terpenoid synthesis as well as the CBB cycle, lower glycolysis and the light-dependent reactions of photosynthesis to enhance squalene production. Additionally, an increased regeneration of the cofactor CTP and a decreased ATP/NADPH ratio are predicted to positively correlate with squalene synthesis. Subsequently, we systematically overexpressed 11 selected targets.

### Systematic overexpression study confirms predictions of FSEOF through altered squalene and pigment content

To test the predictions made by the FBA modeling, 11 genes of interest were inducibly overexpressed in *Synechocystis*  $\Delta$ shc markerless deletion mutant (Dietsch et al., 2021) using the previously characterized rhamnose-inducible promoter system

(Behle et al., 2020) including all genes of the MEP-pathway except for *dxr*, which was previously reported to negatively impact terpenoid production upon overexpression (Choi et al., 2016). In addition to genes directly involved in terpenoid synthesis, *gap2*, *pyrK* and *tpi* were overexpressed to increase availability of pyruvate and G3P. All strains, including the control and wild type possessed the pSHDY *rhaS* replicative plasmid. *Synechocystis Δshc* pSHDY *rhaS* serves as the control due to its ability to accumulate squalene. The functionality of the overexpression system was confirmed by performing qRT-PCR on two representative genes, showing increased transcript levels upon induction (Figure S4 (SI)).

The experimental work showed that squalene production was increased, albeit in some cases only slightly compared to the *Δshc* strain for all overexpressed genes identified by FSEOF, as shown in Figure 2. The amounts of squalene produced in these strains vary widely, depending on the overexpressed gene (Table S4 (SI)).

Overexpression of genes strongly altered the pigmentation in several strains, with the relative changes compared to the *Synechocystis Δshc* control strain shown in Figure 3. Growth was slightly reduced in the overexpression strains, as shown in Figure S5 (SI).

Most overexpression strains showed a reduction in chlorophyll and carotenoid content, as shown in Figure 3 likely due to

disruption of optimal pigment synthesis caused by genetic modification, leading to accumulation of metabolites which may inhibit enzymes upstream in their respective pathway. The reduction in pigments may also be caused by the presence of an additional antibiotic resistance cassette in the overexpression strains. However, the strong pigment variations between overexpression mutants suggest only a weak effect of the antibiotic compared to the genetic change. The overexpression of *ispE*, *ispH* and *gap2* are notable exceptions to this observation, showing little changes in pigmentation upon overexpression. Absorbance spectra of all strains can be seen in Figure S6 (SI). The overexpression of *sqs* led to a blue-colored phenotype, which is characterized by reduced chlorophyll and strongly reduced carotenoid concentrations, as shown in Figure 4.

## Overexpression of *sqs* is the most effective way to improve squalene production

In the MEP pathway, overexpression of *dxs* did not have a strong effect on squalene production, shown in Figure 2, while the downstream reactions catalyzed by IspD, IspE, IspF and IspH

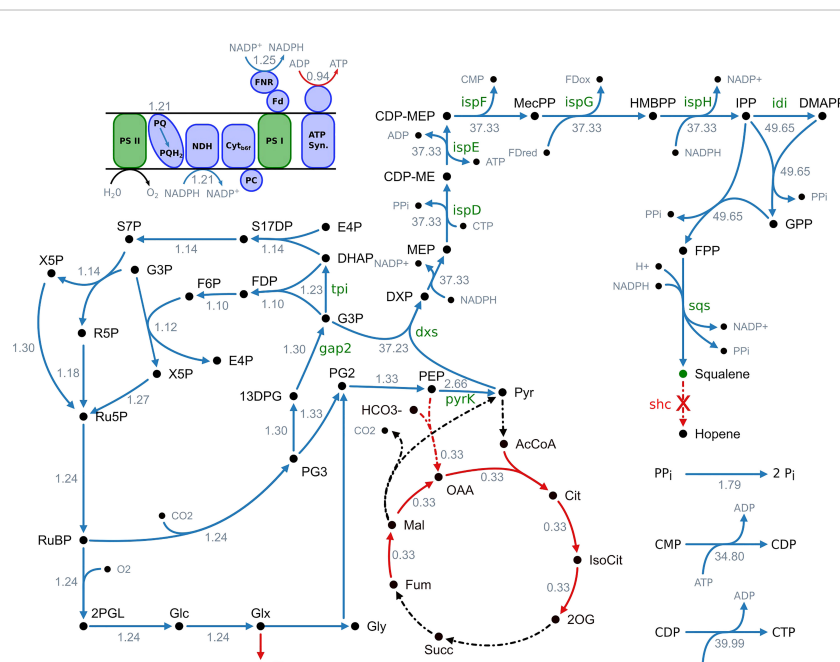


FIGURE 1

Overview of fluxes predicted to change upon increased squalene production. Blue arrows indicate an increased flux and red arrows a decreased flux, respectively. Black arrows indicate no change. Reactions with no flux have a dotted line. The numbers indicate the maximum fold change of the corresponding flux. It is stated that this is not a minimal network but a part of the genome-scale model and not all active reactions are shown. 13DPG, 1;3-bisphosphoglycerate; 2OG, 2-oxoglutarate; 2PGL, 2-phosphoglycolate; AcCoA, acetyl-CoA; ATP synth., ATP synthase; CDP-ME, 4-(cytidine 5'-diphospho)-2-C-methyl-D-erythritol; CDP-MEP, 2-phospho-4-(cytidine 5'-diphospho)-2-C-methyl-D-erythritol; DXP, 1-deoxy-D-xylulose 5-phosphate; E4P, erythrose 4-phosphate; F6P, fructose 6-phosphate;  $Fd_{ox}$ , ferredoxin (oxidized);  $Fd_{red}$ , ferredoxin (reduced); FDP, fructose 1;6-biphosphate; FNR, ferredoxin-NADP<sup>+</sup> reductase; FPP, farnesyl pyrophosphate; Fum, fumarate; G3P, glyceraldehyde 3-phosphate; Glc, D-glycose; Glx, glyoxylate; Gly, glycolate; GPP, geranyl pyrophosphate; HMBPP, 1-hydroxy-2-methyl-2-(E)-butenyl 4-diphosphate; IsoCit, isocitrate; IPP, isopentenyl diphosphate; Mal, malonate; MecPP, 2-C-methyl-D-erythritol 2;4-cyclodiphosphate; MEP, 2-C-methyl-D-erythritol 4-phosphate; NDH, NADPH dehydrogenase; OAA, oxaloacetate; PC, plastocyanin; PEP, phosphoenolpyruvate; PG2, 2-phosphoglycerate; PG3, 3-phosphoglycerate; Pi, orthophosphate; PPI, diphosphate; PQ, plastoquinone; PQH<sub>2</sub>, plastoquinone; PSI, photosystem I; PSII, photosystem II; Pyr, pyruvate; R5P, ribose 5-phosphate; Ru5P, ribulose 5-phosphate; RuBP, ribulose 1;5-biphosphate; S17DP, sedoheptulose 1;7-bisphosphate; S7P, sedoheptulose 7-phosphate; Succ, succinate; X5P, xylulose 5-phosphate.

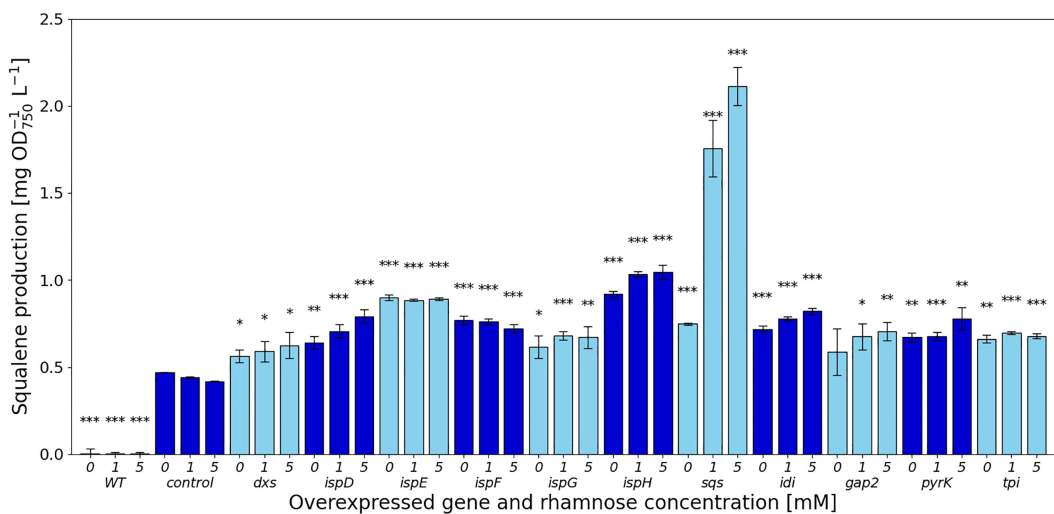


FIGURE 2

Squalene concentrations [ $\text{mg l}^{-1} \text{OD}_{750}^{-1}$ ] in response to gene overexpressions. Values are represented as the means of three biological replicates, standard deviations are shown. WT represents the *Synechocystis* sp. PCC 6803 wild type, while the control strain is *Synechocystis* sp. PCC 6803  $\Delta$ shc pSHDY *rhaS*, from which the overexpression strains were constructed by inserting an additional copy of the specified gene under the control of the rhamnose-inducible promoter  $P_{\text{rha}}$  into its genome. Asterisks (\*) represent the p-value of the two-sided t-test between the respective strain and the control strain at the same rhamnose concentration (\* denotes a value of  $p < 0.05$ , \*\* denotes  $p < 0.01$  and \*\*\* denotes  $p < 0.001$ ). Samples were measured after three days of incubation with the specified concentration of rhamnose as an inducer.

showed more positive effects. The overexpression of both *ispE* and *ispH* led to increased squalene production, even without any inducer present, suggesting that the leakiness of the rhamnose promoter provided sufficient additional enzyme to relieve a bottleneck from the MEP pathway. Overexpressing *ispD* on the other hand increased squalene concentrations in a more concentration-dependent manner. Overexpression of *ispG* did not increase squalene content by a large amount, also showing the strongest negative impact on pigment concentrations of the overexpression of genes in the MEP pathway.

The overexpression of *idi* increased squalene concentrations by 1.96-fold, reducing pigment concentrations in the process, likely by shifting the IPP/DMAPP ratio.

The overexpression of *sqs* led to a 5-fold increased squalene concentration, yielding  $2.11 \text{ mg OD}_{750}^{-1} \text{l}^{-1}$ . *Synechocystis*' SqS may be a particularly active enzyme, as cloning in *E. coli* proved challenging, possibly due to toxicity of squalene to *E. coli*, limiting cell densities in liquid culture and favoring mutated or truncated versions of the gene on agar plates. *E. coli* DH5 $\alpha$  cells transformed with a non-mutated version of *sqs* typically required around 36 h of incubation at  $37^\circ\text{C}$  to form colonies of normal size. The overexpression of *sqs* led to a decrease in chlorophyll and a strong decrease in carotenoid content in *Synechocystis*, as shown by its cell absorbance spectrum in Figure 4.

Of the genes not involved in terpenoid synthesis, overexpressing *gap2*, a central enzyme involved in the CBB cycle only led to a small increase in squalene concentrations, but did so while keeping pigment concentrations approximately at the same level as in the  $\Delta$ shc base strain. Upon induction, squalene and pigment content increased with the inducer concentration. Overexpression of *pyrK*, a glycolysis gene, increased squalene concentrations after induction, but reduced pigment concentrations. Expression of *tpi* did not have

a strong positive effect on squalene concentrations and also reduced pigmentation.

The strain overexpressing *sqs* was additionally investigated regarding its squalene production in 30 ml Erlenmeyer flasks, with its growth and squalene production over time shown in Figure 5. The yield of the culture after 14 days was  $2.78 \text{ mg l}^{-1} \text{ OD}_{750}^{-1}/13.72 \text{ mg l}^{-1}$ .

In summary, all overexpression strains showed increased squalene production, with the overexpression of *sqs* leading to a 5-fold improvement compared to the base strain, with longer term cultivation leading to a yield of  $13.72 \text{ mg l}^{-1}$ . The most efficient overexpressions regarding squalene yield were all in the MEP-pathway and terpenoid synthesis, but overexpression of *gap2* was also notable, as it showed a positive impact on both pigment and squalene concentrations with increasing induction.

## Discussion

In the pursuit of identifying potential amplification targets, improving cyanobacterial squalene production upon upregulation, we used a genome scale constraint-based metabolic model. Twelve of the identified overexpression targets were experimentally confirmed.

The analysis suggested an up-regulation of fluxes through the MEP pathway and terpenoid synthesis. Since terpenoids are exclusively synthesized via the MEP pathway in *Synechocystis*, this is very intuitive and shows the robustness of our *in silico* analysis pipeline. Flux through the light-dependent reactions of photosynthesis as well as the CBB cycle were proposed to increase, to meet the demand of fixed carbon and produce the cofactor NADPH. In fact, the FNR reaction showed an increased flux, while the ATPase reaction is proposed to be downregulated,

leading to an overall decreased ATP/NADPH ratio. Previous *in silico* studies suggested lower ATP/NADPH ratio requirements for many biofuels as well (Erdrich et al., 2014; Shabestary and Hudson, 2016; Englund et al., 2018). Artificially creating imbalances in this ratio could increase product formation. This can be achieved via different approaches, e.g., by blocking cyclic and other alternative electron flows. As a result, ATP and NADPH are forced to be synthesized exclusively via linear electron flow, whose ATP/NADPH ratio is below the ratio required for biomass synthesis. Knocking out ATP producing reactions or introducing ATP futile cycles or other waste reactions could force the organism to use terpenoid production as a sink for excess reduction equivalents (Erdrich et al., 2014). The carboxylation and oxygenation reaction of RuBisCO were coupled in our model, so the flux through the photorespiratory reactions was forced to increase as well. The model suggested using the glycerate photorespiratory bypass. Nonetheless, since it is an undesired reaction to occur, we did not consider it as an amplification target. On the contrary, Zhou et al.

could show that impairing photorespiration leads to a redirection of excess energy and isoprene production could be doubled (Zhou et al., 2021). Additionally, cytidine triphosphate (CTP), a cofactor in the MEP pathway, has to be regenerated by multiple phosphorylations of cytidinmonophosphat (CMP) and the model proposed it might become rate limiting upon high squalene flux. Furthermore, the conversion of diphosphate to monophosphate was predicted to be upregulated because of the increased levels of diphosphate released by IspD, CrtE and SqS. These results are in accordance with previous *in silico* studies aiming to increase terpenoid production in cyanobacteria, although different models as well as different algorithms were utilized (Lin et al., 2017; Englund et al., 2018). The TCA cycle was indicated to decrease in flux, since it is a sink for carbon, which also was found by previous studies in cyanobacteria (Englund et al., 2018). This finding is in contrast to studies in *E. coli* (Choi et al., 2010), where the TCA cycle is called to be upregulated. This difference can be explained by the fact that heterotrophs like *E. coli* have to regenerate their cofactors via the TCA cycle and autotrophs, in contrast, are able to generate cofactors via the light reactions of photosynthesis. The metabolic model suggested a decrease in photosynthetic pigments as well, since increased squalene production diverts carbon flux away from pigments and they compete for the precursor GPP (Lin et al., 2017).

Flux variability analysis found 31 fluxes to be consistent with the results of the FSEOF analysis and increase upon enforced squalene flux. Among the remaining eight fluxes, three showed a pattern where the maximum flux decreased, while the minimum flux increased, and were thus not considered as amplification targets (Choi et al., 2010). The reaction catalyzed by Idi was the only one to display a sign change, where the maximum flux is positive and the minimum flux is negative, implicating the direction of the metabolic flux is unknown and cannot be determined by flux variability analysis (Flowers et al., 2018). Incorporating kinetic parameters as constraints would help to increase the accuracy of the prediction (Moulin et al., 2021). Since in either direction, the flux through Idi positively correlates with squalene production, we chose to verify the result experimentally. Four reactions were completely unbound, thus providing no further information. Previous studies (Choi et al., 2010) showed that the overexpression of unbound targets also had a positive impact on product synthesis.

To confirm the predictions made by the FSEOF analysis, 11 genes were experimentally overexpressed in *Synechocystis*  $\Delta shc$ . All overexpression strains showed elevated squalene levels, but the degrees to which squalene concentrations were increased varied widely. Overall, growth of the overexpression strains was slightly reduced compared to the control (Figure S5 (SI)), possibly as a result of the additional antibiotic present in the growth medium. The differences between the overexpression of genes in the MEP pathway are of particular interest, as regulations and feedback mechanisms in the pathway are not entirely known. Since protein tags can affect both activity and stability of enzymes, we chose to use the native protein sequences for overexpression. Since no antibodies are reported for these native enzymes, we were not able to quantify their protein concentrations. However, we confirmed the functionality of our expression system via qRT-PCR for the *dxs* and *sqs* overexpression strains which both showed increased

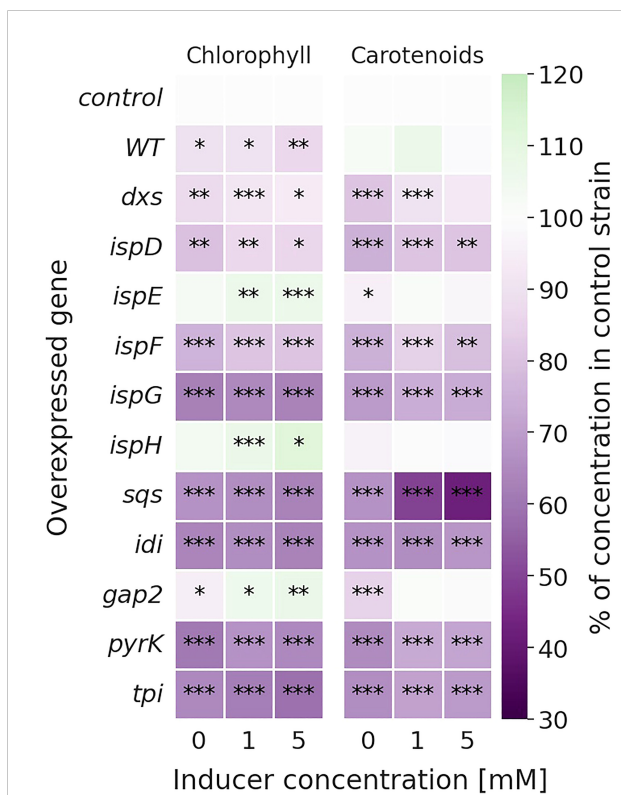


**FIGURE 3**  
Relative change in chlorophyll (left) and carotenoid (right) concentrations [ $\text{mg l}^{-1} \text{OD}_{750}^{-1}$ ] of the overexpression strains compared to the  $\Delta shc$  control strain. Values are represented as the means of three biological replicates. WT represents the *Synechocystis* sp. PCC 6803 wild type, while the control strain is *Synechocystis* sp. PCC 6803  $\Delta shc$  pSHDY *rhaS*, from which the overexpression strains were constructed by inserting an additional copy of the specified gene under the control of the rhamnose-inducible promoter  $P_{rha}$  into its genome. Asterisks (\*) represent the *p*-value of the two-sided t-test between the respective strain and the control strain at the same rhamnose concentration (\* denotes a value of  $p < 0.05$ , \*\* denotes  $p < 0.01$  and \*\*\* denotes  $p < 0.001$ ). Samples were measured after three days of incubation with the specified concentration of rhamnose as an inducer.

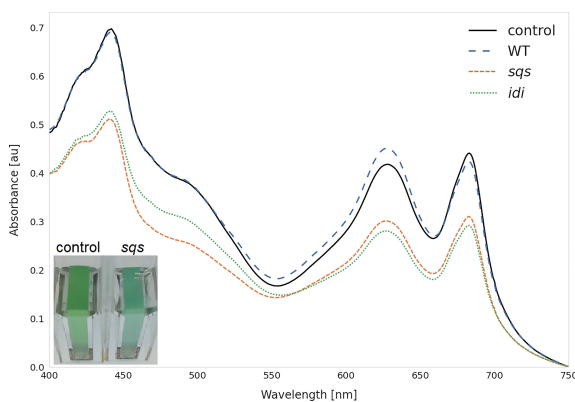


FIGURE 4

Whole cell spectra of selected strains. Spectra were measured after three days incubation with 5 mM rhamnose in 1 cm cuvettes after equalizing the OD<sub>750</sub> across all strains and subtracting the OD<sub>750</sub> as a baseline correction. WT represents the *Synechocystis* sp. PCC 6803 wild type, while the control strain is *Synechocystis* sp. PCC 6803 Δshc pSHDY *rhaS*, from which the overexpression strains were constructed. The visually blue phenotype of the *sqs* overexpression strain in the cuvette is pictured in the bottom left.

transcript levels upon induction with rhamnose (Figure S4 (SI)). Quantitative differences in RNA abundance between genes are unavoidable due to differing mRNA lengths and stabilities, but it can be safely assumed that induction of expression through addition of rhamnose yields higher gene expression levels than the control in all cases. Since no protein amounts could be quantified in this study, no conclusions can be drawn regarding the metabolic efficiency of each overexpression relative to the expression strength. Instead, changes in the final metabolite concentrations are caused by the combined effect of the strength of the overexpression and the catalytic activity of the protein.

*Dxs* is reported to be the rate limiting enzyme of the MEP pathway in many previous studies, but did not prove to be a particularly beneficial overexpression target in this study. This may be attributed to the native *Sqs* activity not providing a strong

enough carbon sink downstream of the MEP pathway, leading to the accumulation of intermediates, such as IPP and DMAPP, which are reported to act as inhibitors to the *Dxs* enzyme (Banerjee et al., 2013; Álvarez-Vasquez et al., 2021; Di et al., 2022). Kudoh et al., 2017 showed that overexpression of *dxs* led to aggregation of the inactivated protein via allosteric inhibition by IPP and DMAPP, ultimately diminishing the impact of the overexpression on the protein level (Kudoh et al., 2017). Protein inactivation may also explain the small effect of *dxs* overexpression on metabolites in this study.

Other studies reported MEcPP to accumulate upon overexpression of *dxs*, so a dual overexpression with *ispG* may show a more positive effect (Gao et al., 2016; Volke et al., 2019). The overexpression of *ispG* alone did not lead to increased production however, the dependence of IspG on reduced ferredoxin units may be a limiting factor to the conversion of MEcPP to HMBPP (Wang and Oldfield, 2014). If the concentrations of MEcPP were too low for IspG to be limiting, the binding of ferredoxin to the additional enzyme may be the cause of the reduction in photosynthetic pigments, with the overexpression of *ispG* leading to the lowest chlorophyll concentrations among the genes of the MEP pathway.

In contrast to most overexpressions, *ispE* and *ispH* showed a positive effect on squalene production even without inducer present, but not strongly increasing upon induction. This relationship suggests that these enzymatic steps represent a metabolite bottleneck, which can be relieved through a slight overexpression and then yields diminishing returns upon stronger overexpression.

The overexpression of *idi* led to an increase in squalene while decreasing pigments, which is in accordance with the predictions made by the constraint-based model. IspH favors production of IPP from HMBPP over DMAPP, while Idi favors the isomerization of IPP towards DMAPP, leading to an IPP : DMAPP ratio of 3:1 *in vivo*, the optimal ratio for production of GGPP (Chaves et al., 2016; Volke et al., 2019). The overexpression of *idi* likely shifted the IPP : DMAPP ratio in favor of DMAPP.

Overexpressing *sqs* led to the strongest increase in squalene and reduction in carotenoids. *Sqs* competes with the native GGPP synthase *crtE* for the intermediate FPP, with the overexpression leading to a shift in favor of squalene, away from GGPP, the precursor for carotenoids and phytol. Since there was only little change in growth over three days (Figure S5 (SI)), the reduced pigmentation did not seem to have a significant negative effect on the cell, but shifting the balance further towards squalene might lead to decreased photosynthetic performance. Overexpression of *ispH* and *ispE* on the other hand increased squalene concentrations as well as the total amount of measured terpenoids, defined as the sum of squalene, carotenoid and the phytol chain of chlorophyll by up to 18%. Combining the overexpressions of *sqs* with *ispH* and *ispE*, may be a promising strategy moving forward, as increased total flux through the MEP pathway can both compensate for the reduced pigmentation caused by *sqs* overexpression and increase squalene titers.

In conclusion, FSEOF allowed us to choose biologically relevant amplification targets computationally, all of which had a positive effect on squalene synthesis upon experimental validation.

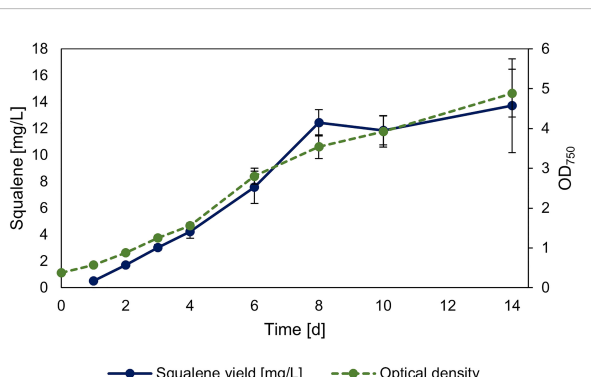


FIGURE 5

Timeseries of squalene production in *sqs* overexpression strain. Squalene production and OD<sub>750</sub> of *Synechocystis* Δshc pEERM P<sub>rha</sub> *sqs* pSHDY *rhaS* in a 30 ml flask culture in mg l<sup>-1</sup> over a period of two weeks after induction with 5 mM rhamnose to trigger overexpression of the squalene synthase (*sqs*). Means and standard deviations of three biological replicates are shown.

Considering squalene is synthesized via the linear MEP pathway, most of the identified targets are rather intuitive. Since we were able to confirm all selected targets, we suggest a validation of the non-intuitive targets outside the MEP pathway, such as Ppa and FNR for further studies. These two targets have previously been predicted and tested in *Synechocystis* (Englund et al., 2018). Our findings propose that constraint-based metabolic models could aid in the selection of targets improving the production of desired metabolites. This could be of particular interest for the prediction of combinatorial interventions. However, classic FBA does not account for regulatory mechanisms like feedback inhibition or potential metabolite toxicity (Knoop and Steuer, 2015). It could be helpful for future studies to test FSEOF in combination with dynamic extensions of FBA (Mahadevan et al., 2002) and hybrid kinetic and constraint-based models (Shameer et al., 2022). The incorporation of metabolite concentrations, flux rates or kinetic parameters could drastically improve the precision and reliability of the results (Mahadevan et al., 2002; Moulin et al., 2021; Shameer et al., 2022). For future studies we suggest the combinatorial expression of the identified amplification targets, especially with the native *sqs*, since it seems to be the rate limiting enzyme in the present study, as well as the combination of amplification and knock-down targets. Our experiments are in accordance with the central idea of synthetic biology, where experimental designs are determined by metabolic modeling and experimental results can feed back data into models to increase their accuracy, leading to deterministic, steady improvement. The overexpression of the native *sqs* gene of *Synechocystis* proved to be the most successful strategy for squalene production to date, with the strain reaching a higher production titer than heterologous *sqs* expression in *Synechocystis* (Pattanaik et al., 2020).

## Data availability statement

The original contributions presented in the study are included in the article/[Supplementary Material](#). Further inquiries can be directed to the corresponding author.

## Author contributions

AG: Conceptualization, Investigation, Methodology, Computational work, Writing – Original draft, review & editing, Data Visualization. AN: Conceptualization, Investigation, Experimental work, Writing – Original draft, review & editing, Data Visualization. MD: Conceptualization, Methodology,

Experimental work, Writing – review & editing. TP: Computational work, Writing -Data visualization, review. DM: Experimental work, Writing – Review & Editing. ST: Experimental work, Writing – Review & Editing. PW: Methodology, Data Curation. IA: Supervision, Writing – review & editing. All authors contributed to the article and approved the submitted version.

## Funding

This work was funded by the Deutsche Forschungsgemeinschaft (DFG, German Research Foundation) under Germany's Excellence Strategy – EXC-2048/1 - project ID 390686111, and further, by project ID 391465903/GRK 2466.

## Acknowledgments

We thank Ralf Steuer for the kind provision of the metabolic model. We also thank Anna Behle for the pSHDY plasmid and for assistance with the design of genetic constructs, as well as Pia Lindberg for providing the pEERM4 plasmid.

## Conflict of interest

The authors declare that the research was conducted in the absence of any commercial or financial relationships that could be construed as a potential conflict of interest.

## Publisher's note

All claims expressed in this article are solely those of the authors and do not necessarily represent those of their affiliated organizations, or those of the publisher, the editors and the reviewers. Any product that may be evaluated in this article, or claim that may be made by its manufacturer, is not guaranteed or endorsed by the publisher.

## Supplementary material

The Supplementary Material for this article can be found online at: <https://www.frontiersin.org/articles/10.3389/fpls.2023.1024981/full#supplementary-material>

## References

Álvarez-Vasquez, F., González-Alcón, C., Gallego-Jara, J., de Diego, T., Cánovas, M., and Torres, N. V. (2021). Model based optimization of the terpenoids biosynthesis in *E. coli*. *bioRxiv*. doi: 10.1101/2021.08.11.455928

Banerjee, A., Wu, Y., Banerjee, R., Li, Y., Yan, H., and Sharkey, T. D. (2013). Feedback inhibition of deoxy-D-xylulose-5-phosphate synthase regulates the methylerythritol 4-phosphate pathway. *J. Biol. Chem.* 288, 16926–16936. doi: 10.1074/jbc.M113.464636

- Barone, G. D., Cernava, T., Ullmann, J., Liu, J., Lio, E., Germann, A. T., et al. (2023). Recent developments in the production and utilization of photosynthetic microorganisms for food applications. *Heliyon* 9 (4). doi: 10.1016/j.heliyon.2023.e14708
- Bhatia, A., Bharti, S. K., Tewari, S. K., Sidhu, O. P., and Roy, R. (2013). Metabolic profiling for studying chemotype variations in *Withania somnifera* (L.) Dunal fruits using GC-MS and NMR spectroscopy. *Phytochemistry* 93:105–115. doi: 10.1016/j.phytochem.2013.03.013
- Behle, A., Saake, P., Germann, A. T., Dienst, D., and Axmann, I. M. (2020). Comparative dose-response analysis of inducible promoters in cyanobacteria. *ACS Synth. Biol.* 9, 843–855. doi: 10.1021/acssynbio.9b00505
- Bennett, A., and Bogorad, L. (1973). Complementary chromatic adaptation in a filamentous blue-green alga. *J. Cell Biol.* 58, 419–435. doi: 10.1083/jcb.58.2.419
- Berla, B. M., Saha, R., Immethun, C. M., Maranas, C. D., Moon, T. S., and Pakrasi, H. B. (2013). Synthetic biology of cyanobacteria: unique challenges and opportunities. *Front. Microbiol.* 4. doi: 10.3389/fmib.2013.00246
- Brodrick, J. T., Rubin, B. E., Welkie, D. G., Du, N., Mih, N., Diamond, S., et al. (2016). Unique attributes of cyanobacterial metabolism revealed by improved genome-scale metabolic modeling and essential gene analysis. *Proc. Natl. Acad. Sci. U. S. A.* 113, E8344–E8353. doi: 10.1073/pnas.1613446113
- Burgard, A. P., Pharkya, P., and Maranas, C. D. (2003). OptKnock: a bilevel programming framework for identifying gene knockout strategies for microbial strain optimization. *Biotechnol. Bioeng.* 84, 647–657. doi: 10.1002/bit.10803
- Chaves, J. E., Romero, P. R., Kirst, H., and Melis, A. (2016). Role of isopentenyl-diphosphate isomerase in heterologous cyanobacterial (*Synechocystis*) isoprene production. *Photosynth. Res.* 130, 517–527. doi: 10.1007/s11120-016-0293-3
- Choi, S. Y., Lee, H. J., Choi, J., Kim, J., Sim, S. J., Um, Y., et al. (2016). Photosynthetic conversion of CO<sub>2</sub> to farnesyl diphosphate-derived phytochemicals (amorphadiene and squalene) by engineered cyanobacteria. *Biotechnol. Biofuels* 9, 202. doi: 10.1186/s13068-016-0617-8
- Choi, H. S., Lee, S. Y., Kim, T. Y., and Woo, H. M. (2010). In silico identification of gene amplification targets for improvement of lycopene production. *Appl. Environ. Microbiol.* 76, 3097–3105. doi: 10.1128/AEM.00115-10
- Choi, S. Y., Sim, S. J., Ko, S. C., Son, J., Lee, J. S., Lee, H. J., et al. (2020). Scalable cultivation of engineered cyanobacteria for squalene production from industrial flue gas in a closed photobioreactor. *J. Agric. Food Chem.* 68, 10050–10055. doi: 10.1021/acs.jafc.0c03133
- Choi, S. Y., Wang, J. Y., Kwak, H. S., Lee, S. M., Um, Y., Kim, Y., et al. (2017). Improvement of squalene production from CO<sub>2</sub> in *Synechococcus elongatus* PCC 7942 by metabolic engineering and scalable production in a photobioreactor. *ACS Synth. Biol.* 6, 1289–1295. doi: 10.1021/acssynbio.7b00083
- Connolly, J. D., and Hill, R. A. (2010). Triterpenoids. *Nat. Prod. Rep.* 27, 79–132. doi: 10.1039/b808530g
- Di, X., Ortega-Alarcon, D., Kakumanu, R., Iglesias-Fernandez, J., Diaz, L., Baiddoo, E. K., et al. (2022). MEP pathway products allosterically promote monomerization of deoxy-D-xylulose-5-phosphate synthase to feedback-regulate their supply. *Plant Commun.*, 100512. doi: 10.1016/j.xplc.2022.100512
- Dietsch, M., Behle, A., Westhoff, P., and Axmann, I. M. (2021). Metabolic engineering of *Synechocystis* sp. PCC 6803 for the photoproduction of the sesquiterpene valencene. *Metab. Eng. Commun.* 13, e00178. doi: 10.1016/j.mec.2021.e00178
- Ebrahim, A., Lerman, J. A., Palsson, B. O., and Hyduke, D. R. (2013). COBRApy: COnstraints-based reconstruction and analysis for Python. *BMC Syst. Biol.* 7, 74. doi: 10.1186/1752-0509-7-74
- Englund, E., Andersen-Ranberg, J., Miao, R., Hamberger, B., and Lindberg, P. (2015). Metabolic engineering of *Synechocystis* sp. PCC 6803 for production of the plant diterpenoid manoyl oxide. *ACS Synth. Biol.* 4, 1270–1278. doi: 10.1021/acssynbio.5b00070
- Englund, E., Pattanaik, B., Ubhayasekera, S. J. K., Stensjö, K., Bergquist, J., and Lindberg, P. (2014). Production of squalene in *Synechocystis* sp. PCC 6803. *PLoS One* 9 (3), e90270. doi: 10.1371/journal.pone.0090270
- Englund, E., Shabestary, K., Hudson, E. P., and Lindberg, P. (2018). Systematic overexpression study to find target enzymes enhancing production of terpenes in *Synechocystis* PCC 6803, using isoprene as a model compound. *Metab. Eng.* 49, 164–177. doi: 10.1016/j.ymben.2018.07.004
- Erdrich, P., Knoop, H., Steuer, R., and Klamt, S. (2014). Cyanobacterial biofuels: new insights and strain design strategies revealed by computational modeling. *Microb. Cell Fact.* 13, 128. doi: 10.1186/s12934-014-0128-x
- Flowers, J. J., Richards, M. A., Baliga, N., Meyer, B., and Stahl, D. A. (2018). Constraint-based modelling captures the metabolic versatility of *Desulfovibrio vulgaris*. *Environ. Microbiol. Rep.* 10, 190–201. doi: 10.1111/1758-2229.12619
- Gao, X., Gao, F., Liu, D., Zhang, H., Nie, X., and Yang, C. (2016). Engineering the methylerythritol phosphate pathway in cyanobacteria for photosynthetic isoprene production from CO<sub>2</sub>. *Energy Environ. Sci.* 9, 1400–1411. doi: 10.1039/c5ee03102h
- Gohil, N., Bhattacharjee, G., Khambhati, K., Braddick, D., and Singh, V. (2019). Engineering strategies in microorganisms for the enhanced production of squalene: advances, challenges and opportunities. *Front. Bioeng. Biotechnol.* 7. doi: 10.3389/fbioe.2019.00050
- Hays, S. G., and Ducat, D. C. (2015). Engineering cyanobacteria as photosynthetic feedstock factories. *Photosynth. Res.* 123, 285–295. doi: 10.1007/s11120-014-9980-0
- He, H.-P., Corke, H., and Cai, J.-G. (2003). Supercritical carbon dioxide extraction of oil and squalene from amaranthus grain. *J. Agric. Food Chem.* 51, 7921–7925. doi: 10.1021/jf030488y
- Hellier, P., Al-Haj, L., Talibi, M., Purton, S., and Ladommato, N. (2013). Combustion and emissions characterization of terpenes with a view to their biological production in cyanobacteria. *Fuel* 111, 670–688. doi: 10.1016/j.fuel.2013.04.024
- Hemmerlin, A., Tritsch, D., Hartmann, M., Pacaud, K., Hoeffler, J. F., van Dorsselaer, A., et al. (2006). A cytosolic *Arabidopsis* d-xylulose kinase catalyzes the phosphorylation of 1-deoxy-D-xylulose into a precursor of the plastidial isoprenoid pathway. *Plant Physiol.* 142 (2), 441–457. doi: 10.1104/pp.106.086652
- Hendry, J. I., Bandyopadhyay, A., Srinivasan, S., Pakrasi, H. B., and Maranas, C. D. (2020). Metabolic model guided strain design of cyanobacteria. *Curr. Opin. Biotechnol.* 64, 17–23. doi: 10.1016/j.copbio.2019.08.011
- Ho, H.-M., Huang, C.-Y., Cheng, Y.-J., Shen, K.-Y., Tzeng, T.-T., Liu, S.-J., et al. (2021). Assessment of adjuviant strategy of lipid squalene nanoparticles for enhancing the immunogenicity of a SARS-CoV-2 spike subunit protein against COVID-19. *Int. J. Pharm.* 607, 121024. doi: 10.1016/j.ijpharm.2021.121024
- Hudson, P., Lee, S. Y., Nielsen, J., and Stephanopoulos, G. (2021). *Cyanobacteria biotechnology* (Weinheim, Germany: Wiley-VCH Verlag).
- Jain, S., Prajapat, G., Abrar, M., Ledwani, L., Singh, A., and Agrawal, A. (2017). Cyanobacteria as efficient producers of mycosporine-like amino acids. *J. Basic Microbiol.* 57, 715–727. doi: 10.1002/jobm.201700044
- Kaneko, T., Sato, S., Kotani, H., Tanaka, A., Asamizu, E., Nakamura, Y., et al. (1996). Sequence analysis of the genome of the unicellular cyanobacterium *Synechocystis* sp. strain PCC6803. II. sequence determination of the entire genome and assignment of potential protein-coding regions. *DNA Res.* 3, 109–136. doi: 10.1093/dnares/3.3.109
- Karunanithi, P. S., and Zerbe, P. (2019). Terpene synthases as metabolic gatekeepers in the evolution of plant terpenoid chemical diversity. *Front. Plant Sci.* 10. doi: 10.3389/fpls.2019.01166
- Katabami, A., Li, L., Iwasaki, M., Furabayashi, M., Saito, K., and Umeno, D. (2015). Production of squalene by squalene synthases and their truncated mutants in *Escherichia coli*. *J. Biosci. Bioeng.* 119, 165–171. doi: 10.1016/j.jbiosc.2014.07.013
- King, Z. A., Lloyd, C. J., Feist, A. M., and Palsson, B. O. (2015). Next-generation genome-scale models for metabolic engineering. *Curr. Opin. Biotechnol.* 35, 23–29. doi: 10.1016/j.copbio.2014.12.016
- Klaus, O., Hilgers, F., Nakielski, A., Hasenklever, D., Jaeger, K.-E., Axmann, I. M., et al. (2022). Engineering phototrophic bacteria for the production of terpenoids. *Curr. Opin. Biotechnol.* 77, 102764–102022. doi: 10.1016/j.copbio.2022.102764
- Knoop, H., and Steuer, R. (2015). A computational analysis of stoichiometric constraints and trade-offs in cyanobacterial biofuel production. *Front. Bioeng. Biotechnol.* 3. doi: 10.3389/fbioe.2015.00047
- Kohno, Y., Egawa, Y., Itoh, S., Nagaoka, S.-I., Takahashi, M., and Mukai, K. (1995). Kinetic study of quenching reaction of singlet oxygen and scavenging reaction of free radical by squalene in n-butanol. *Biochim. Biophys. Acta (BBA) - Lipids Lipid Metab.* 1256, 52–56. doi: 10.1016/0005-2760(95)00005-w
- Kudoh, K., Hotta, S., Sekine, M., Fujii, R., Uchida, A., Kubota, G., et al. (2017). Overexpression of endogenous 1-Deoxy-D-Xylulose 5-phosphate synthase (DXS) in cyanobacterium *Synechocystis* sp. PCC6803 accelerates protein aggregation. *J. Biosci. Bioeng.* 123 (5), 590–596. doi: 10.1016/j.jbiosc.2017.01.001
- Lau, N.-S., Matsui, M., and Abdullah, A. A.-A. (2015). Cyanobacteria: photoautotrophic microbial factories for the sustainable synthesis of industrial products. *Biomed. Res. Int.* 2015, 754934. doi: 10.1155/2015/754934
- Leplat, C., Champeimont, R., Saenham, P., Cassier-Chauvat, C., Jean-Christophe, A., and Chauvat, F. (2013). Genome-wide transcriptome analysis of hydrogen production in the cyanobacterium *Synechocystis*: towards the identification of new players. *Int. J. Hydrogen Energy* 38, 1866–1872. doi: 10.1016/j.ijhydene.2012.11.118
- Liang, Z., Zhu, H., Wang, X., Jing, B., Li, Z., Xia, X., et al. (2020). Adjuvants for coronavirus vaccines. *Front. Immunol.* 11. doi: 10.3389/fimmu.2020.589833
- Lin, P.-C., Saha, R., Zhang, F., and Pakrasi, H. B. (2017). Metabolic engineering of the pentose phosphate pathway for enhanced limonene production in the cyanobacterium *Synechocystis* sp. PCC 6803. *Sci. Rep.* 7, 17503. doi: 10.1038/s41598-017-17831-y
- Lin, P.-C., Saha, R., Zhang, F., and Pakrasi, H. B. (2017). Metabolic engineering of the pentose phosphate pathway for enhanced limonene production in the cyanobacterium *Synechocystis* sp. PCC 6803. *Sci. Rep.* 7, 17503. doi: 10.1038/s41598-017-17831-y
- Lichtenthaler, H. K., and Buschmann, C. (2001). Chlorophylls and carotenoids: Measurement and characterization by UV-VIS spectroscopy. *Curr. Protoc. Food Anal. Chem.* 1, F4.3.1–F4.3.8. doi: 10.1002/0471142913.faf0403s01
- Mahadevan, R., Edwards, J. S., and Doyle, F. J. 3rd (2002). Dynamic flux balance analysis of diauxic growth in *Escherichia coli*. *Biophys. J.* 83, 1331–1340. doi: 10.1016/S0006-3495(02)73903-9
- Mendes, A., Azevedo-Silva, J., and Fernandes, J. C. (2022). From sharks to yeasts: squalene in the development of vaccine adjuvants. *Pharmaceuticals* 15 (3), 265. doi: 10.3390/ph15030265

- Moss, G. P., Smith, P. A. S., and Tavernier, D. (1995). Glossary of class names of organic compounds and reactivity intermediates based on structure (IUPAC Recommendations 1995). *J. Macromol. Sci. Part A Pure Appl. Chem.* 67, 1307–1375. doi: 10.1351/pac199567081307
- Moulin, C., Tournier, L., and Peres, S. (2021). Combining kinetic and constraint-based modelling to better understand metabolism dynamics. *Processes* 9, 1701. doi: 10.3390/pr9101701
- Mulkidjanian, A. Y., Koonin, E. V., Makarova, K. S., Mekhedov, S. L., Sorokin, A., Wolf, Y. I., et al. (2006). The cyanobacterial genome core and the origin of photosynthesis. *Proc. Natl. Acad. Sci. U.S.A.* 103, 13126–13131. doi: 10.1073/pnas.0605709103
- O'Hagan, D. T., van der Most, R., Lodaya, R. N., Coccia, M., and Lofano, G. (2021). "World in motion" - emulsion adjuvants rising to meet the pandemic challenges. *NPJ Vaccines* 6, 158. doi: 10.1038/s41541-021-00418-0
- Okada, K., and Hase, T. (2005). Cyanobacterial non-mevalonate pathway: (E)-4-hydroxy-3-methylbut-2-enyl diphosphate synthase interacts with ferredoxin in *Thermosynechococcus elongatus* BP-1. *J. Biol. Chem.* 280, 20672–20679. doi: 10.1074/jbc.M500865200
- Oliver, J. W. K., and Atsumi, S. (2015). A carbon sink pathway increases carbon productivity in cyanobacteria. *Metab. Eng.* 29, 106–112. doi: 10.1016/j.ymben.2015.03.006
- Oliver, N. J., Rabinovitch-Deere, C. A., Carroll, A. L., Nozzi, N. E., Case, A. E., and Atsumi, S. (2016). Cyanobacterial metabolic engineering for biofuel and chemical production. *Curr. Opin. Chem. Biol.* 35, 43–50. doi: 10.1016/j.cbpa.2016.08.023
- Park, S. Y., Binkley, R. M., Kim, W. J., Lee, M. H., and Lee, S. Y. (2018). Metabolic engineering of *Escherichia coli* for high-level astaxanthin production with high productivity. *Metab. Eng.* 49, 105–115. doi: 10.1016/j.ymben.2018.08.002
- Pattanaik, B., Englund, E., Nolte, N., and Lindberg, P. (2020). Introduction of a green algal squalene synthase enhances squalene accumulation in a strain of *Synechocystis* sp. PCC 6803. *Metab. Eng. Commun.* 10, e00125. doi: 10.1016/j.mec.2020.e00125
- Pils, D., and Schmetterer, G. (2001). Characterization of three bioenergetically active respiratory terminal oxidases in the cyanobacterium *Synechocystis* sp. strain PCC 6803. *FEMS Microbiol. Lett.* 203, 217–222. doi: 10.1111/j.1574-6968.2001.tb10844.x
- Pinto, F. L., Thapper, A., Sontheim, W., and Lindblad, P. (2009). Analysis of current and alternative phenol based RNA extraction methodologies for cyanobacteria. *BMC Molecular Biol.* 10, 79. doi: 10.1186/1471-2199-10-79
- Posten, C., and Schaub, G. (2009). Microalgae and terrestrial biomass as source for fuels—a process view. *J. Biotechnol.* 142, 64–69. doi: 10.1016/j.jbiotec.2009.03.015
- Pulz, O., and Gross, W. (2004). Valuable products from biotechnology of microalgae. *Appl. Microbiol. Biotechnol.* 65, 635–648. doi: 10.1007/s00253-004-1647-x
- Raman, K., and Chandra, N. (2009). Flux balance analysis of biological systems: applications and challenges. *Brief. Bioinform.* 10, 435–449. doi: 10.1093/bib/bbp011
- Ramey, C. J., Barón-Sola, Á., Aucoin, H. R., and Boyle, N. R. (2015). Genome engineering in cyanobacteria: where we are and where we need to go. *ACS Synth. Biol.* 4, 1186–1196. doi: 10.1021/acssynbio.5b00043
- Rippka, R., Stanier, R. Y., Deruelles, J., Herdman, M., and Waterbury, J. B. (1979). Generic assignments, strain histories and properties of pure cultures of cyanobacteria. *Microbiology* 111, 1–61. doi: 10.1099/00221287-111-1-1
- Ronco, A. L., and De Stefani, E. (2013). Squalene: a multi-task link in the crossroads of cancer and aging. *Funct. Foods Health Dis.* 3, 462. doi: 10.31989/ffhd.v3i12.30
- Satoh, S., Ikeuchi, M., Mimuro, M., and Tanaka, A. (2001). Chlorophyll b expressed in cyanobacteria functions as a light-harvesting antenna in photosystem I through flexibility of the proteins. *J. Biol. Chem.* 276, 4293–4297. doi: 10.1074/jbc.M008238200
- Sawai, S., and Saito, K. (2011). Triterpenoid biosynthesis and engineering in plants. *Front. Plant Sci.* 2. doi: 10.3389/fpls.2011.00025
- Schellenberger, J., Que, R., Fleming, R. M. T., Thiele, I., Orth, J. D., Feist, A. M., et al. (2011). Quantitative prediction of cellular metabolism with constraint-based models: the COBRA toolbox v2.0. *Nat. Protoc.* 6, 1290–1307. doi: 10.1038/nprot.2011.308
- Schirrmeister, B. E., de Vos, J. M., Antonelli, A., and Bagheri, H. C. (2013). Evolution of multicellularity coincided with increased diversification of cyanobacteria and the great oxidation event. *Proc. Natl. Acad. Sci. U.S.A.* 110, 1791–1796. doi: 10.1073/pnas.1209927110
- Segrè, D., Vitkup, D., and Church, G. M. (2002). Analysis of optimality in natural and perturbed metabolic networks. *Proc. Natl. Acad. Sci. U.S.A.* 99, 15112–15117. doi: 10.1073/pnas.232349399
- Shabestary, K., and Hudson, E. P. (2016). Computational metabolic engineering strategies for growth-coupled biofuel production by *Synechocystis*. *Metab. Eng. Commun.* 3, 216–226. doi: 10.1016/j.meteno.2016.07.003
- Shameer, S., Wang, Y., Bota, P., Ratcliffe, R. G., Long, S. P., and Sweetlove, L. J. (2022). A hybrid kinetic and constraint-based model of leaf metabolism allows predictions of metabolic fluxes in different environments. *Plant J.* 109, 295–313. doi: 10.1111/tpj.15551
- Shen, C. R., and Liao, J. C. (2013). Synergy as design principle for metabolic engineering of 1-propanol production in *Escherichia coli*. *Metab. Eng.* 17, 12–22. doi: 10.1016/j.ymben.2013.01.008
- Smith, T. J., Yang, G. Y., Seril, D. N., Liao, J., and Kim, S. (1998). Inhibition of 4-(methylnitrosamino)-1-(3-pyridyl)-1-butane-induced lung tumorigenesis by dietary olive oil and squalene. *Carcinogenesis* 19, 703–706. doi: 10.1093/carcin/19.4.703
- Steuer, R., Knoop, H., and Machné, R. (2012). Modelling cyanobacteria: from metabolism to integrative models of phototrophic growth. *J. Exp. Bot.* 63, 2259–2274. doi: 10.1093/jxb/ers018
- St. John, P. (2016). "d3flux," in *Openbase*. Available at: <https://openbase.com/python/d3flux>
- Volke, D. C., Rohwer, J., Fischer, R., and Jennewein, S. (2019). Investigation of the methylerythritol 4-phosphate pathway for microbial terpenoid production through metabolic control analysis. *Microb. Cell Fact.* 18, 1–15. doi: 10.1186/s12934-019-1235-5
- Wang, W., and Oldfield, E. (2014). Bioorganometallic chemistry with IspG and IspH: structure, function, and inhibition of the [Fe(4)S(4)] protein involved in isoprenoid biosynthesis. *Angew. Chem. Int. Ed. Engl.* 53, 4294–4310. doi: 10.1002/anie.201306712
- Xu, R., Fazio, G. C., and Matsuda, S. P. T. (2004). On the origins of triterpenoid skeletal diversity. *Phytochemistry* 65, 261–291. doi: 10.1016/j.phytochem.2003.11.014
- Yang, Y.-F., Jan, Y.-H., Liu, Y.-P., Yang, C.-J., Su, C.-Y., Chang, Y.-C., et al. (2014). Squalene synthase induces tumor necrosis factor receptor 1 enrichment in lipid rafts to promote lung cancer metastasis. *Am. J. Respir. Crit. Care Med.* 190, 675–687. doi: 10.1164/rccm.201404-0714OC
- Zhou, J., Yang, F., Zhang, F., Meng, H., Zhang, Y., and Li, Y. (2021). Impairing photorespiration increases photosynthetic conversion of CO<sub>2</sub> to isoprene in engineered cyanobacteria. *Bioresources Bioprocessing* 8, 1–13. doi: 10.1186/s40643-021-00398-y